PHYSICAL REVIEW B **91**, 195424 (2015)

# Kondo effect in binuclear metal-organic complexes with weakly interacting spins

L. Zhang,[1,2] A. Bagrets,[1] D. Xenioti,[3,1] R. Korytár,[1] M. Schackert,[2] T. Miyamachi,[2,4] F. Schramm,[1] O. Fuhr,[1]
R. Chandrasekar,[5] M. Alouani,[3] M. Ruben,[1,3] W. Wulfhekel,[2,1] and F. Evers[6,1]
[1]*Institute of Nanotechnology, Karlsruhe Institute of Technology (KIT), 76021 Karlsruhe, Germany*
[2]*Physikalisches Institut, Karlsruhe Institute of Technology (KIT), 76021 Karlsruhe, Germany*
[3]*Institut de Physique et Chimie des Matériaux de Strasbourg (IPCMS), 67034 Strasbourg, France*
[4]*Institute of Solid State Physics, University of Tokyo, Kashiwa, Chiba 277-8581, Japan*
[5]*School of Chemistry, University of Hyderabad, 500 046 Hyderabad, India*
[6]*Institut für Theorie der Kondensierten Materie, Karlsruhe Institute of Technology, 76021 Karlsruhe, Germany*
(Received 23 September 2014; published 18 May 2015)

We report a combined experimental and theoretical study of the Kondo effect in a series of binuclear metal-organic complexes of the form $[(\mathrm{Me(hfacac)_2})_2(\mathrm{bpym})]^0$, with Me = nickel (II), manganese (II), zinc (II); hfacac = hexafluoroacetylacetonate, and bpym = bipyrimidine, adsorbed on Cu(100) surface. While Kondo features did not appear in the scanning tunneling spectroscopy spectra of nonmagnetic $\mathrm{Zn_2}$, a zero bias resonance was resolved in magnetic $\mathrm{Mn_2}$ and $\mathrm{Ni_2}$ complexes. The case of $\mathrm{Ni_2}$ is particularly interesting as the experiments indicate two adsorption geometries with very different properties. For $\mathrm{Ni_2}$ complexes we have employed density functional theory to further elucidate the situation. Our simulations show that one geometry with relatively large Kondo temperatures $T_\mathrm{K} \sim 10$ K can be attributed to distorted $\mathrm{Ni_2}$ complexes, which are chemically bound to the surface via the bipyrimidine unit. The second geometry we assign to molecular fragmentation: we suggest that the original binuclear molecule decomposes into two pieces, including Ni(hexafluoroacetylacetonate)$_2$, when brought into contact with the Cu substrate. For both geometries our calculations support a picture of the ($S = 1$)-type Kondo effect emerging due to open $3d$ shells of the individual $\mathrm{Ni^{2+}}$ ions.

DOI: 10.1103/PhysRevB.91.195424 PACS number(s): 81.07.Nb, 68.37.Ef, 75.76.+j, 31.15.E−

## I. INTRODUCTION

Molecular electronics holds the vision that functional electronic devices, like memory elements, rectifiers, and transistors, may be realized by designing suitable molecular complexes. Over the past decade, two- and three-terminal molecular junctions with current-voltage characteristics resembling diod- [1,2], transistor- [3–5], or memorylike [6,7] behavior have been demonstrated. The function of molecular devices can be extended using the spin degree of freedom initiating the field of molecular spintronics. An important step in this direction was made recently, when a giant magnetoresistance effect has been demonstrated for single molecules deposited on a ferromagnetic surface [8,9].

In order to achieve external control of electron spins, "spin-transition" complexes have been proposed, which can be addressed by temperature, pressure, light, and presumably electron charging [10–12]. In these systems a *single spin* is the main protagonist. When it is brought in contact with a substrate, the Kondo effect sets in. It has been observed in systems with increasing complexity ranging from $3d$ or $4f$ adatoms on metallic surfaces [13–18], through molecules with extended $\pi$ orbitals [19–22], to carbon nanotubes [23,24].

The motivation of our work is the question of what happens if the molecule approaching the surface has *more* than a single active spin, say two exchange coupled spins that anticipate the case of single molecule magnets (SMMs) [25]. Interesting new aspects can enter already on the level of binuclear magnets [33,34] and arise from the competition of substrate effects, such as Kondo screening, and the intermolecular exchange coupling.

Motivated by such a question, we have synthesized a series of binuclear metal-organic complexes of the form $[(\mathrm{Me(hfacac)_2})_2(\mathrm{bpym})]^0$, referred to later on as "$\mathrm{Me_2}$" (see Fig. 1). These complexes have been deposited on a clean Cu(001) surface and studied with low-temperature scanning tunneling microscopy (STM). While no feature of the Kondo effect was found in the scanning tunneling spectroscopy (STS) spectrum of $\mathrm{Zn_2}$ with closed-shell $3d$ ions, an adsorption-site dependent zero-bias (Kondo) resonance was clearly resolved in the case of $\mathrm{Mn_2}$ and $\mathrm{Ni_2}$ molecules (see Fig. 2).

The $\mathrm{Ni_2}$ case is particularly interesting, as the adsorbed molecule appears in two variants that differ in STM images and STS characteristics. To rationalize these observations, we have performed calculations based on density functional theory (DFT). We thus identify possible adsorption geometries. Our simulations show that one observed geometry (with relatively large Kondo temperature $T_\mathrm{K}$) can be attributed to the original $\mathrm{Ni_2}$ complex with a distorted geometry bound to Cu(001) via the bipyrimidine (bpym) unit. The other is likely to arise from molecular fragmentation. We propose that upon approaching the substrate the molecule breaks and forms two $\mathrm{Ni(hfacac)_2}$ moieties, which are then seen in the experiment.

## II. SYNTHESIS AND CHARACTERIZATION OF BINUCLEAR COMPLEXES

*Molecular geometries.* The molecular structure of the neutral binuclear metal complexes $[(\mathrm{Me(hfacac)_2})_2(\mathrm{bpym})]^0$, with Me = nickel (II), manganese (II), zinc (II); hfacac = hexafluoroacetylacetonate, and bpym = bipyrimidine, studied in this work is presented in Fig. 1. The structural details of the metal complexes, in particular the coordination environment of the metal ions, are sensitive to the kind of $3d$ metal ion involved (for details, see the Supplemental Material [35], Sec. IV). According to single-crystal x-ray diffractometry [46] each

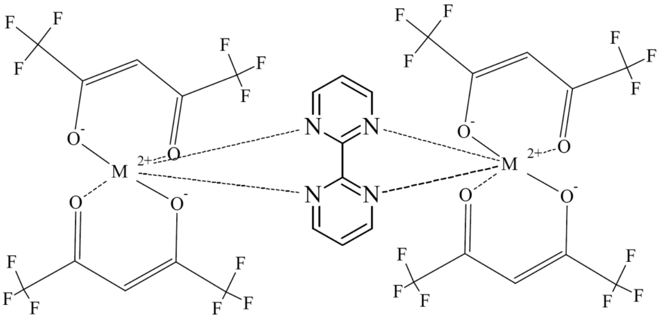

FIG. 1. Structure of the $(Me(hfacac)_2)_2(bpym)$ complex. Each metal ion $Me^{2+}$ is linked with two hexafluoroacetylacetonate (hfacac) ligands by Me-O bonds. By forming N-Me bonds the aromatic 2,2'-bipyrimidine (bpym) ligand coordinates as bidentate chelate with two of the $Me(hfacac)_2$ components.

$Mn^{2+}$ ion is situated in a distorted trigonal prismatic $N_2O_4$ coordination sphere leading to a Mn-Mn distance of 6.2 Å in $Mn_2$ dimer. By contrast, the $Ni_2$ complex exhibits a distorted octahedral coordination environment of each $Ni^{2+}$ ion [47] with a Ni-Ni distance of only 5.6 Å.

*Magnetism.* The magnetic behavior of polycrystalline samples of the $Mn_2$ and $Ni_2$ complexes was determined between 2 and 300 K (Supplemental Material [35], Sec. IV). At room temperature $Mn_2$ has a $\chi_M T$ value of 9.03 $\text{cm}^3\,\text{K}\,\text{mol}^{-1}$ (here $\chi_M$ is the molar magnetic susceptibility and $T$ is the temperature), corresponding to two uncoupled high-spin Mn(II) ions with a spin value of $S = 5/2$ each, while $Ni_2$ shows a $\chi_M T$ product of 2.23 $\text{cm}^3$ K $\text{mol}^{-1}$, corresponding to two uncoupled Ni(II) ions with $S = 1$. Between 300 and 75 K both the $Mn_2$ and $Ni_2$ complexes show paramagnetic behavior, while below 75 K weak antiferromagnetic (AF) behavior sets in. The AF exchange interaction between the two divalent $3d$ ions through a bpym bridging ligand is reported as $J_{\text{ex}}^{\text{AF}} = 1.6$ meV [48] and $J_{\text{ex}}^{\text{AF}} = 2.06$ meV [47] for $Ni_2$, which is about ten times larger than the exchange interaction observed in $Mn_2$ with $J_{\text{ex}}^{\text{AF}} = 0.13$ meV.

*DFT calculations for the* $Ni_2$ *complex.* The spin state of each of the two $Ni(hfacac)_2$ units was determined as $S = 1$ assuming an $[Ar]3d^8$ electronic configuration for the $Ni^{2+}$ ion. Specifically, the atomic structure of the nonadsorbed (gas-phase) $Ni_2$ complex was refined starting from the x-ray-diffraction structure with $Ni^{2+}$ ions in distorted octahedral environment (see Supplemental Material [35], Sec. I, for computational details). The results of the "constrained" DFT calculations are summarized in the first row of Table I. In particular, our calculations predict a "singlet" ground state with the two spins, $S = 1$, coupled antiferromagnetically. For the gas-phase complex, very low excitation energy ($\simeq$15 meV) is observed with an excited state exhibiting ferromagnetic coupling. Our results are consistent with experimental findings: weak antiferromagnetic exchange interaction between the two metal ions of the $[(Me(hfacac)_2)_2(bpym)]^0$ complexes facilitated by the bpym ligand has been reported before [47].

## III. STM EXPERIMENTS

The STM experiments were performed using a home-built, low-noise STM operating between 0.7 and 4.2 K in ultrahigh vacuum (UHV) ($p < 10^{-9}$ mbar) [51]. Clean and atomically flat Cu(100) substrates were prepared *in situ* followed by deposition of molecules by sublimation at 80–100 °C. Three adsorption configurations, $\alpha$ ($Ni_2$ and $Zn_2$), $\beta$ (only $Ni_2$), and $\gamma$ ($Mn_2$ and $Ni_2$), of the molecules on Cu(100) were found [see Figs. 2(a)–2(e)]. Scanning tunneling spectroscopy (STS) measurements were performed on these different configurations. Kondo-like peaks were clearly resolved in the $dI/dU$ curves of $Mn_2$ and $Ni_2$ (in both configurations) near the Fermi level while no remarkable feature was found in the $dI/dU$ curve of the nonmagnetic $Zn_2$ complexes [see spectra displayed in Fig. 2(f)].

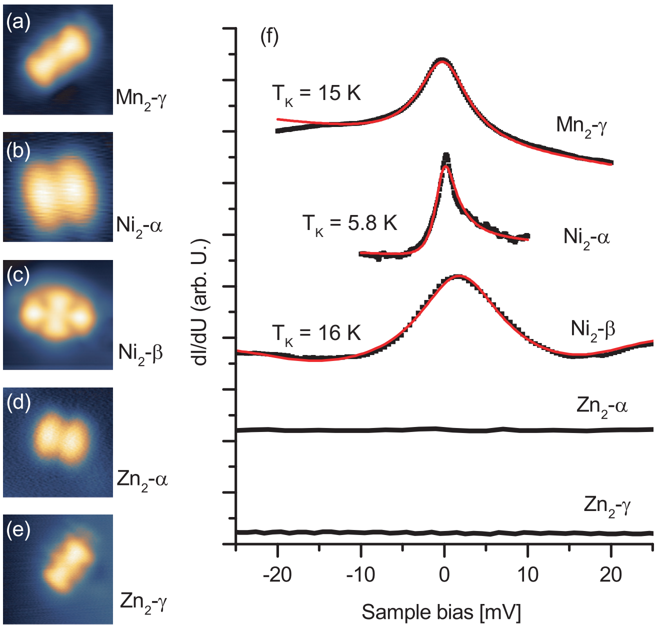

FIG. 2. (Color online) Topography of (a) $Mn_2$-$\gamma$, (b) $Ni_2$-$\alpha$, (c) $Ni_2$-$\beta$, (d) $Zn_2$-$\alpha$, and (e) $Zn_2$-$\gamma$. [Images (a)–(e) are squares of side length of 3.7, 2.8, 2.5, 2,9, and 3.3 nm, respectively. Feedback conditions are 100 mV and 1 nA, 200 mV and 200 pA, −10 mV and 200 pA, 15 mV and 1 nA, 100 mV and 1 nA, respectively.] The orientation of $\beta$ and $\gamma$ configuration follows [001] and [011] direction of the substrate, respectively, while the orientation of $\alpha$ configuration seems to be random. The differential conductance $dI/dU$ near the Fermi level is shown in (f). The black dots are experimental data which were fitted with Fano functions (red lines). The STM images and STS were measured at 4.2 K. The spectra are normalized and a linear background was considered to obtain reasonable fitting result.

The Kondo effect arises when the magnetic moment of an impurity is screened by surrounding electrons of a nonmagnetic substrate [52,53]. As the simplest manifestation of the interaction between the localized spin and delocalized electrons, the shape of the zero-bias anomaly in STS caused by the Kondo effect can be described by a Fano resonance [54–56]:

$$\frac{dI}{dU}(U) \propto \frac{(\varepsilon + q)^2}{1 + \varepsilon^2}, \tag{1}$$

where

$$\varepsilon = \frac{eU - \varepsilon_0}{\Gamma}, \tag{2}$$

TABLE I. Relative energies of the low-energy spin configurations realized in $Ni_2$ complexes, which were estimated based on the ground-state constrained DFT calculations (see Supplemental Material [35] for computational details). Considered molecules are (i) gas-phase relaxed $Ni_2$ complex, with $Ni^{2+}$ ions found in distorted octahedral environment [Suppl. Fig. 1(a)]; (ii) free but distorted $Ni_2$ complex, prerelaxed in the presence of Cu surface, where local $C_{2v}$ symmetry has been kept [Suppl. Fig. 4(a)]; (iii) free but distorted $Ni_2$ complex, relaxed in the presence of Cu surface where symmetry constrains have been released [Suppl. Fig. 4(b)]. Spin configurations labeled as F and AF stand for ferromagnetic (F) and antiferromagnetic (AF) coupling, respectively, between $S = 1$ spins localized on $Ni^{2+}$ ions. Last column refers to magnetically excited zero-spin (closed-shell) state at one of $Ni^{2+}$ ions.

| | DFT implementation | AF: ↑↑↓↓ | F: ↑↑↑↑ | ↑↑↑↓ |
|---|---|---|---|---|
| (i) relaxed $Ni_2$ | FHI-aims [49] | 0.000 eV | 15.8 meV | 0.500 eV |
| complex | TURBOMOLE [50] | 0.000 eV | 14.9 meV | 0.522 eV |
| (ii) distorted $Ni_2$ complex | FHI-aims | 0.000 eV | 6.9 meV | 0.396 eV |
| with $C_{2v}$ symmetry | TURBOMOLE | 0.000 eV | 6.1 meV | 0.390 eV |
| (iii) distorted | FHI-aims | 0.000 eV | 2.5 meV | 0.456 eV |
| $Ni_2$ complex | TURBOMOLE | 0.000 eV | 1.9 meV | 0.361 eV |

and $\varepsilon_0$ is the energy shift of the resonance from the Fermi level, $\Gamma$ is the width of the resonance. The Fano parameter $q$ characterizes the interference of tunneling between the tip and the magnetic impurity and tunneling between the tip and the sample [57]. Considering the temperature dependence, the Kondo resonance can be approximated by a Lorentzian resonance [58]. Thus the energy width $2\Gamma(T)$ (full width at half maximum) of a Kondo resonance can be expressed as

$$2\Gamma(T) = 2\sqrt{(\pi k_B T)^2 + 2(k_B T_K)^2}, \tag{3}$$

with $k_B$ being the Boltzmann constant, $T$ being the environment temperature, and $T_K$ being the Kondo temperature. By fitting the experimental STS with Eqs. (1)–(3), the Kondo temperature $T_K$ is extracted.

The $Zn^{2+}$ ions in the complex are expected to have a full $3d$ subshell, so a magnetic moment is absent. This is in agreement with the superconducting quantum interference device measurements of the crystals of this complex. Thus, a Kondo effect could appear only in adsorbed molecules if a charge transfer between the molecule and the substrate leads to the acquisition of a magnetic moment on the molecule. Since our measurements do not indicate a Kondo resonance [compare Fig. 2(f)], we conclude that the interaction with the substrate is too weak for such a charge transfer. Contrary to $Zn^{2+}$, in $Mn_2$ and $Ni_2$ the central $Mn^{2+}/Ni^{2+}$ ions exhibit a partially filled $3d$ shell and therefore carry a finite magnetic moment. They are at the origin of the Kondo effect that we observe in our measurements, Fig. 2. By fitting to the Fano-shaped resonance, a Kondo temperature of 15 K for $Mn_2$ is determined.

With $Ni_2$ the situation is more complex since two different adsorption geometries (referred to as $\alpha$ and $\beta$) are observed; see Figs. 2(b) and 2(c). We determine two Kondo temperatures, 5.8 and 16 K for $Ni_2$-$\alpha$ and $Ni_2$-$\beta$, respectively. An even clearer difference between these adsorption geometries exhibits itself in a site-dependent STS measurement that we perform on $Ni_2$-$\alpha$ and $Ni_2$-$\beta$; see Fig. 3. The measurement shows that the Kondo resonance has a single maximal amplitude at the center of the $Ni_2$-$\alpha$ complex [cf. Figs. 3(a) and 3(c)], while two spots with maximal amplitude of $dI/dU$ signal separated by a distance of 4 Å are clearly resolved in the STS map of $Ni_2$-$\beta$ [cf. Figs. 3(b) and 3(d)], which match the two $Ni^{2+}$ ions and their expected distance in the molecule.

At first sight, these results suggest that adsorption configurations of $Ni_2$ complexes may look like those shown in Figs. 3(e) and 3(f). Namely, $Ni_2$-$\beta$ could correspond to the molecular complex, which “lies” on the surface with both of its hfacac ligands, thus exposing the two Ni ions separately to the STM tip. The $\alpha$ configuration could correspond to the complex, which “stands” on the surface with one hfacac ligand and the other hfacac ligand is seen in its topographic image. This would expose the two Ni ions above each other such that a single Kondo resonance is observed in STS. As we show later on, the latter assignment is inconsistent with the theoretical considerations. Below, we propose an alternative scenario.

## IV. THEORY

To elucidate microscopic details of the Kondo-effect observed experimentally, we have performed elaborate DFT calculations. Our main objective is to understand the dependence of the Kondo resonance of the $Ni_2$ complex on the adsorption site. Additional questions that we address will concern the nature of molecular orbitals involved in the interaction with conduction electrons, and how delocalized electrons compete for screening of the initially antiferromagnetically coupled spins.

### A. Simple adsorption geometries

We analyze the adsorption geometries schematically illustrated in Figs. 3(e) and 3(f). They exhibit gas-phase $Ni_2$ complexes placed on Cu(001) surface (see Supplemental Material [35], Sec. II A, for computational details). Our simulation results indicate fluorine-copper distances above ~3 Å. This distance implies that a weak van der Waals (vdW) force dominates binding to the surface. There is only a weak hybridization between molecular and substrate states, which translates into narrow molecular resonances, $\Gamma \simeq 10$ meV, as seen from the spectral function $A(E)$ projected on the Ni(II) ion (see Supplemental Material [35], Suppl. Fig. 2). Giving typical parameters of the Anderson model [59] read from $A(E)$, namely, single occupied resonance level width $\Gamma \simeq 10^{-2}$ eV, on-site Coulomb repulsion energy $U \sim 2$ eV, and position of the resonance level $\varepsilon_d \sim U/2 \sim 1$ eV relative

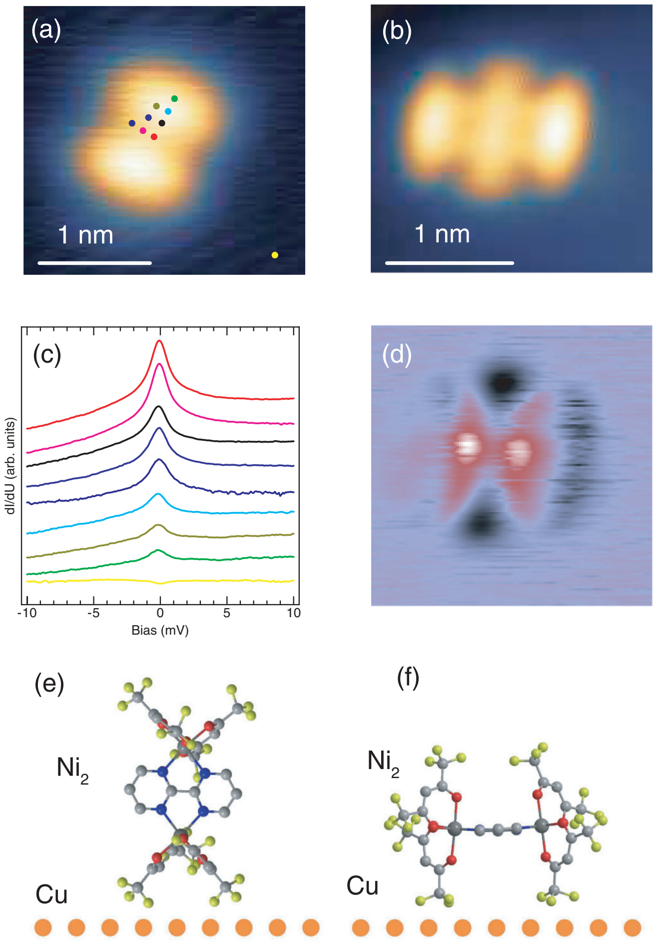

FIG. 3. (Color online) Topography of Ni$_2$-$\alpha$ (a) and Ni$_2$-$\beta$ (b). STS on different position of the Ni$_2$-$\alpha$ is shown in (c) ($T = 1$ K, feedback conditions: $U = 10$ mV, $I = 20$ nA, 200$\mu$V modulation). STS ($dI/dU$) map of Ni$_2$-$\beta$ is shown in (d). White areas indicate large differential conduction, black low ($T = 5$ K, feedback conditions $U = 10$ mV, $I = 10$ nA). An intuitive assumption for the adsorption configurations of Ni$_2$-$\alpha$ and Ni$_2$-$\beta$ (front view) on the Cu(100) substrate is shown in (e) and (f), respectively.

to the Fermi energy, we can estimate the Kondo temperature as [60,61] $k_B T_K \sim U\sqrt{\frac{\Gamma}{4U}}e^{-\pi U/4\Gamma} \sim 0.1e^{-10^2\pi/2}$ eV $\sim 10^{-69}$ eV. This result contradicts the experimental finding of $k_B T_K \sim$ 10 meV, so that we exclude adsorption geometries shown in Figs. 3(e) and 3(f). Alternatives should allow for a stronger binding with a significant amount of hybridization in order to achieve larger $\Gamma$ values.

### B. $\alpha$ configuration: Ni(hfacac)$_2$ fragments on Cu(001)

In order to enforce a much larger coupling of the molecular complex to the substrate we first consider the extreme case of molecular fragmentation; see Fig. 4(a). Here we include the possibility that coordination bonds between the Ni$^{2+}$ ion and nitrogen atoms are broken, and a Ni(hfacac)$_2$ moiety, which is chemically bound to a Cu surface, is observed in the experiment. In that situation the coupling of the spin to the Cu surface is comparable to the case of a single Ni adatom (no ligands attached), and drawing from related earlier experimental experience [16,17,66] one might suspect Kondo temperatures of the order of tenth of meV roughly consistent with the present measurements. In order to show that the fragmentation scenario is consistent with the experimental findings, we observe the following facts:

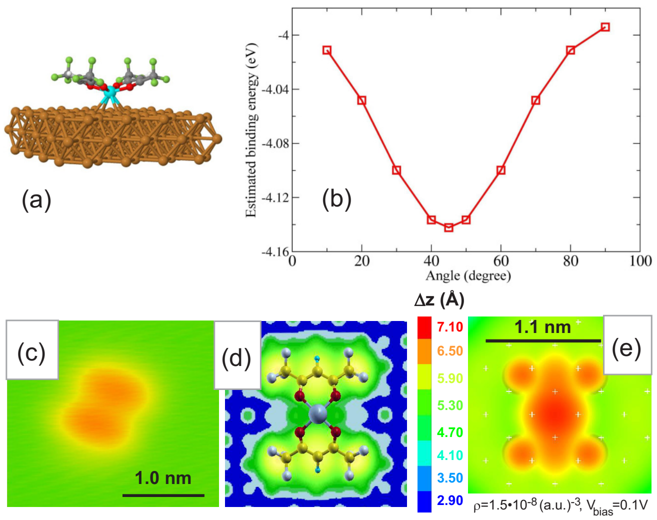

FIG. 4. (Color online) (a) Ni(hfacac)$_2$ moiety bound to a Cu(001) surface via a Ni atom placed at the *hollow* site. (b) Estimated dependence of the binding energy of Ni(hfacac)$_2$ to Cu (001) surface, including contributions due to vdW forces [62], on the angle that fixes the orientation of the moiety's mirror planes vs the [001] direction of the fcc (001) surface. (c) Experimentally recorded topographic Ni$_2$-$\alpha$ STM image (reproduced from Fig. 2), where color coding is identical to Fig. 4(e). (d) Simulated image of Ni(hfacac)$_2$, computed employing VASP package [63]: different colors refer to isosurfaces of the space-resolved (local) density of states (DOS) at the Fermi level. (e) Simulated image of Ni(hfacac)$_2$, computed employing AITRANSS package [64,65]: selected three-dimensional isosurface of the space-resolved DOS (above the molecule) integrated over the energy window 0.1 eV around the Fermi level is shown, where color coding refers to the distance $\Delta z$ to the Cu surface. Consistent with experimental STM image, simulated images obey two mirror planes and outermost contours with a butterfly shape.

(i) *Simulated STM-images.* Our simulations of fragmented molecules [Figs. 4(d) and 4(e)] yield STM images reproducing the most important characteristics of the experimental ones for Ni$_2$-$\alpha$: the outermost contours have a butterfly shape, two mirror planes exist, the size of experimental and computational images are consistent. It is encouraging to see that also nontrivial details are (partially) reproduced. Namely, theory predicts a nonzero optimal angle, 45° [Fig. 4(b)] that fixes orientation of the fragment's mirror planes vs the fcc [100] direction of the (001) surface plane (see also Supplemental Material [35], Suppl. Fig. 3). A nonzero angle, ≈25°, is also observed in the representative experimental images of Ni$_2$-$\alpha$ (see Suppl. Fig. 5).

(ii) *Spatial dependency of Kondo amplitude.* The fragment's geometry is such that the associated Kondo resonance would have maximum amplitude with the STM tip located in the center of the image (at the Ni atom). That is consistent with the structure of the spatially resolved Kondo resonance of Ni$_2$-$\alpha$ observed experimentally [cf. Figs. 2(a) and 2(c)].

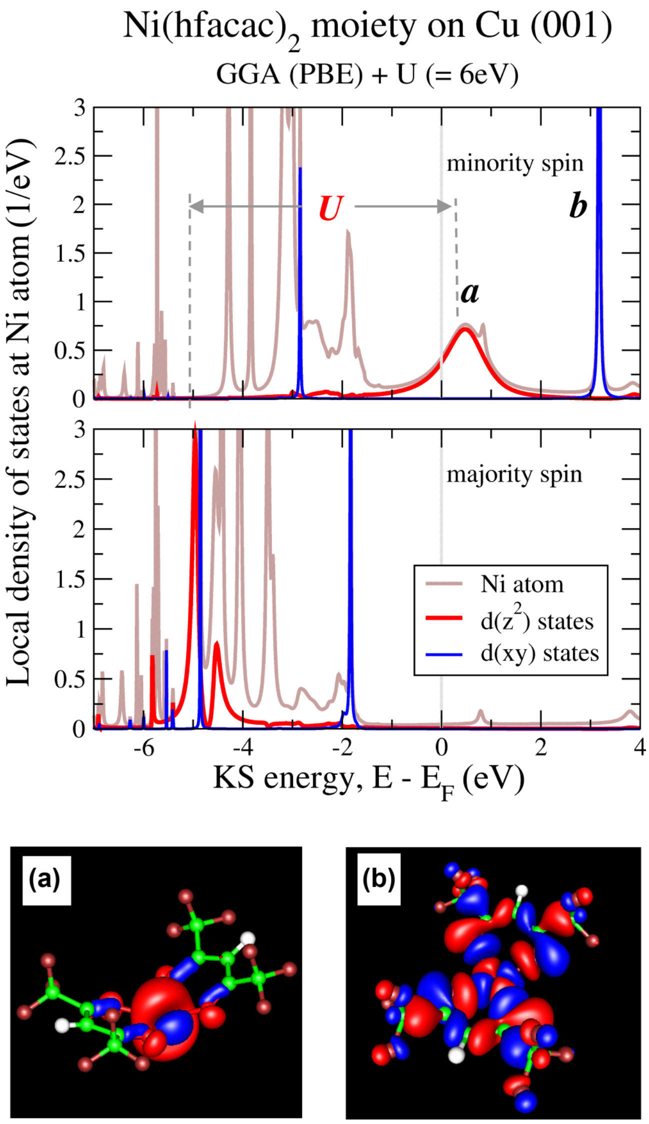

FIG. 5. (Color online) Upper plot: spin dependent local density of states projected on Ni atom of the Ni(hfacac)$_2$ on Cu(001). Red and blue lines highlight contributions to the LDOS associated with Ni $d_{z^2}$ and $d_{xy}$ orbitals. Lower plots: corresponding Kohn-Sham wave functions of the free standing molecule.

(iii) *The effect of temperature on the adsorption.* Experimental STM images characterizing adsorption of Ni$_2$ complexes on Cu(001) surface (Suppl. Fig. 5) suggest that molecular fragmentation at surface is likely triggered by the temperature. Namely, experimental data (Suppl. Fig. 5) reveal that when Ni$_2$ complexes are evaporated on the substrates at room temperature, two species—Ni$_2$-$\alpha$ and Ni$_2$-$\beta$—are found, while Ni$_2$-$\alpha$, which we attribute to molecular fragments, is not found after deposition onto precooled substrates (77 K).

Since the fragmentation scenario is consistent with the experimental phenomenology, we perform further *ab initio* calculations with the goal to better understand the molecular magnetism and eventually estimate the Kondo temperature.

We consider the atomic configuration of Ni atom as [Ar]$4s^2 3d^8$. In the simplified picture of a free Ni(hfacac)$_2$ fragment, the $4s$ states hybridize so strongly with the ligands, that the $s$ electrons are effectively transferred to ligand orbitals. Therefore, the metal ion takes the Ni$^{2+}$ configuration and exhibits two unpaired spins. We performed a DFT study within the generalized gradient approximation (GGA, Perdew-Burke-Ernzerhof exchange-correlation functional [67]) of the molecule in gas phase (for details, see Supplemental Material [35], Sec. I). Our results confirm the above picture: we find a spin-polarized ground state with a magnetic moment of $2\mu_B$. The magnetization is largely due to two orbitals ($a$ and $b$ in Fig. 5) that are populated with up-spin electrons, only, and that contribute substantial weight to both Ni $d_{z^2}$ and $d_{xy}$ atomic states.

One may ask whether the fragment keeps its magnetic moment when adsorbed on the substrate. To answer this question, we performed another spin-DFT study, whose details are presented in the Supplemental Material [35] (Sec. II and Suppl. Fig. 3). In essence, the substrate further breaks the residual degeneracy of the $d$ orbitals splitting $d_{z^2}$ and $d_{xy}$ by 1.4 eV. As a result, $d_{z^2}$ is nearly full (0.4 eV below $E_\mathrm{F}$), while $d_{xy}$ is nearly empty (1 eV above $E_\mathrm{F}$ with resonance $\Gamma_b \approx 10^{-2}$ eV). The magnetization drops after adsorption by about a factor of 2, down to $1.2\mu_B$. The net charge(electron)-transfer to the molecule in the adsorption process is $0.4e$.

The GGA-type calculation leaves us with a situation where a localized $3d_{z^2}$-type orbital is only partially occupied. In DFT with conventional local exchange-correlation (XC) functionals (local-density approximation, GGA) this is typically an indication of correlation physics, such as the Coulomb blockade. The Coulomb blockade is not described by conventional DFT functionals, but it can be captured on the level of GGA+$U$ [68,69]. Therefore, following Ref. [70], we performed a GGA+$U$ calculation placing a repulsive on-site term with (relatively large) strength $U = 6$ eV on the metal site. (Details of our implementation are given in Ref. [71].) The interaction shifts the spin-down resonance $a$ from 0.4 eV below to 0.5 eV above $E_F$ (Fig. 5). Hence, the magnetic moment increases up to $1.62\mu_B$ thus suggesting the picture of the ($S = 1$) Kondo effect.

So far our *ab initio* study has ignored the spatial structure of the two molecular orbitals involved, orbital $a$ with substantial contribution from Ni $d_{z^2}$ atomic state, and orbital $b$ with substantial contribution from Ni $d_{xy}$ atomic state. These molecular orbitals are depicted in Fig. 5. As can be seen, the $a$ orbital (first quantum dot, $\Gamma_a$) is directed towards the surface. Hence, it hybridizes with the substrate much stronger than the $b$ orbital (second dot $\Gamma_b$), i.e., $\Gamma_b \ll \Gamma_a$. Each level has a single occupancy and the electrons populating them are coupled ferromagnetically. Since the exchange interaction ($\sim$0.5 eV, see Table I) is much larger compared to the expected Kondo energy scale $\sim$10 K, both spins form a triplet, $S = 1$. Reading parameters from the spectral function (Fig. 5),

$$\Gamma_a \simeq 0.8 \text{ eV} \gg \Gamma_b; \quad \varepsilon_d \simeq 0.5 \text{ eV}; \quad U \simeq 5.5 \text{ eV} \gg \varepsilon_d,$$

and using a formula [60,61] for the Kondo temperature,

$$k_B T_\mathrm{K} \simeq 0.41\, U \sqrt{\frac{\Gamma^*}{4U}}\, e^{-\pi\varepsilon_d/\Gamma^*}, \tag{4}$$

where $U \gg \varepsilon_d$ and $\Gamma^* = \Gamma_a/2$ for the case of the double-dot system, we obtain $k_B T_\mathrm{K} \simeq 5.84 \times 10^{-3}$ eV, i.e., a

Kondo-temperature $\simeq 70$ K in qualitative agreement with the experiment.

We emphasize that a more precise estimation of the Kondo temperature is hampered by exponential dependence of $T_K$ on model parameters. For example, taking into account that DFT has a tendency to overestimate resonance linewidths, we may assume a slightly smaller $\Gamma_a \simeq 0.6$ eV. This reduces $T_K$ down to $\simeq 16$ K, which is in good agreement with the experimentally observed value.

### C. $\beta$ configuration: Distorted $Ni_2$ complex on Cu(001)

Spatially resolved intensity of the Kondo resonance, measured on top of the $Ni_2$-$\beta$ image [Fig. 3(d)] suggests that also molecular species with two metal ions are to be found on a Cu surface. To rationalize this observation, we performed numerical simulations, to find an intact but strongly distorted molecular conformation [see Fig. 6(g)] that establishes a chemical bond to the Cu surface—an important prerequisite for observable Kondo temperatures. This bond is presumably realized via the delocalized $\pi$ orbitals of the central bpym unit overlapping with the electron density extending from the surface. The bond involves contributions of the vdW forces [62], which have been accounted for in our simulations, and presumably has ionic character due to fractional charge transfer to the quasidegenerate lowest unoccupied molecular orbitals (LUMOs) [72].

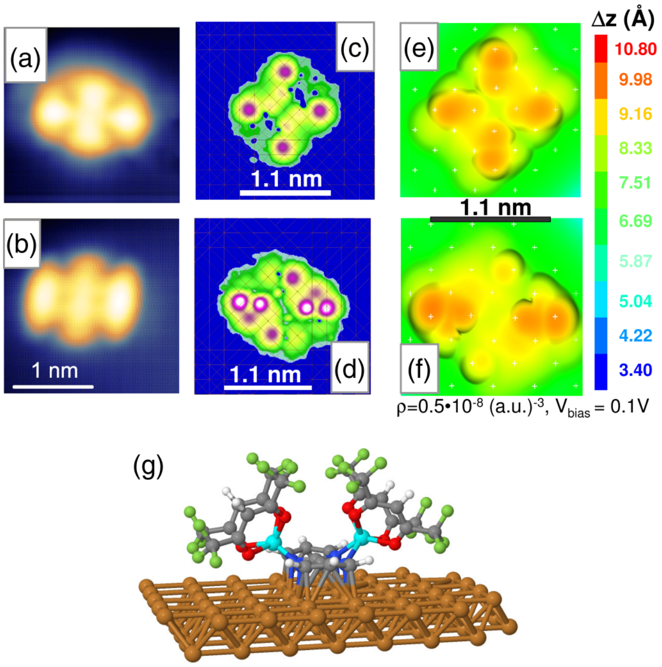

FIG. 6. (Color online) Experimentally recorded (a), (b) $Ni_2$-$\beta$ and simulated STM images of the $Ni_2$ complex, with partially weakened chemical bonds, bound to Cu(001) via the bpym moiety [see lower plot (g)]. Theoretical images are computed with VASP [63] (c),(d) and AITRANSS [65] (e),(f). Images (c) and (e) are obtained assuming symmetry constrains within the DFT relaxation procedure, while images (d) and (f) correspond to the relaxed structure without constrains (see text for further details). Lower plot (g) shows distorted $Ni_2$ complex with partially weakened chemical bonds bound to Cu(001) via (bpym) moiety.

We mention that even for the modern *ab initio* methods, finding the relaxed ground-state structure of a large organic molecule (such as $Ni_2$ complex) on a surface is a nontrivial procedure. Due to the many atomic degrees of freedom involved, relaxation can end up in different molecular conformations with energies differing by $\sim 100$ meV, as was also the case in our simulations. To be specific in the following discussion, we focus on two representative but slightly different conformations of "distorted" $Ni_2$ complex (for details, see Suppl. Fig. 4).

The first conformation [see Suppl. Fig. 4(a)] has been obtained within the preliminary DFT relaxation procedure: the atomic structure of the complex has an (approximate) $C_{2v}$ symmetry, in registry with the underlying fcc(001) surface. For this conformation, the simulated STM image of the complex reveals a "crosslike" structure, resembling $Ni_2$-$\beta$ experimental images [see Figs. 6(a), 6(c), and 6(e)]. Further relaxation steps within the simulation account for an energy gain of about $\sim 0.25$ eV: the local symmetry of the molecular complex is broken resulting in the second conformation [see Suppl. Fig. 4(b)]. Then formerly symmetric simulated crosslike STM images are transformed to the ones with broken symmetry [cf. Figs. 6(d) and 6(f)], which were also experimentally observed [cf. Fig. 6(b)].

The structure of the binuclear complex suggests that the molecular spins should reside on the $Ni(hfacac)_2$ units, where each unit could accept two unpaired electrons (referred to as $S = 1$) owing to $[Ar]3d^8$ electronic configuration of the $Ni^{2+}$ ion. Essentially, the two $S = 1$ subsystems are magnetically nearly decoupled, since only a weak indirect ("superexchange") interaction between them could be realized via the $\pi$ orbitals of the bpym unit. Thus, we anticipate that each subsystem will develop a Kondo effect, independently, as the molecular complex provides two parallel conduction paths (channels) for the tunneling electron, one for each spin.

These expectations are fully confirmed by our computational analysis. Constrained DFT calculations (see data in Table I) predict a "singlet" ground state with antiferromagnetically (AF) coupled $S = 1$ spins. For the distorted $Ni_2$ complex, the state with ferromagnetically (F) coupled $S = 1$ spins is only $\sim 2$ meV above the AF state.

The frontier molecular orbitals (see Fig. 7, bottom panels) carry unpaired spins (ferromagnetic coupling between $S = 1$ subsystems is considered there) confirming the above picture: two out of four orbitals, $a$ and $b$, are primarily localized on the left-hand side of the $Ni_2$ complex, while their counterparts, $a'$ and $b'$, are localized on the right-hand side. When the $Ni_2$ complex is brought in contact with the Cu surface, these molecular orbitals are transformed to resonances $(a,b,a',b')$ in the spectral function centered around $-1.5$ eV below the Fermi level $E_F$ (see Fig. 7), while the upper Hubbard band $(\varepsilon_d)$ is placed just above $E_F$. Furthermore, since the wave functions $a$ and $a'$ involve larger contributions from $\pi$ orbitals of the central bpym unit, the corresponding resonances $a$ and $a'$ are much broader than the $b$ and $b'$ ones.

Assuming that the weak AF coupling between the two subsystems is below the Kondo temperature, $J_{AF} = (E_{AF} - E_F)/2 \simeq 12\text{ K} \leqslant T_K$ (otherwise the AF singlet ground state would

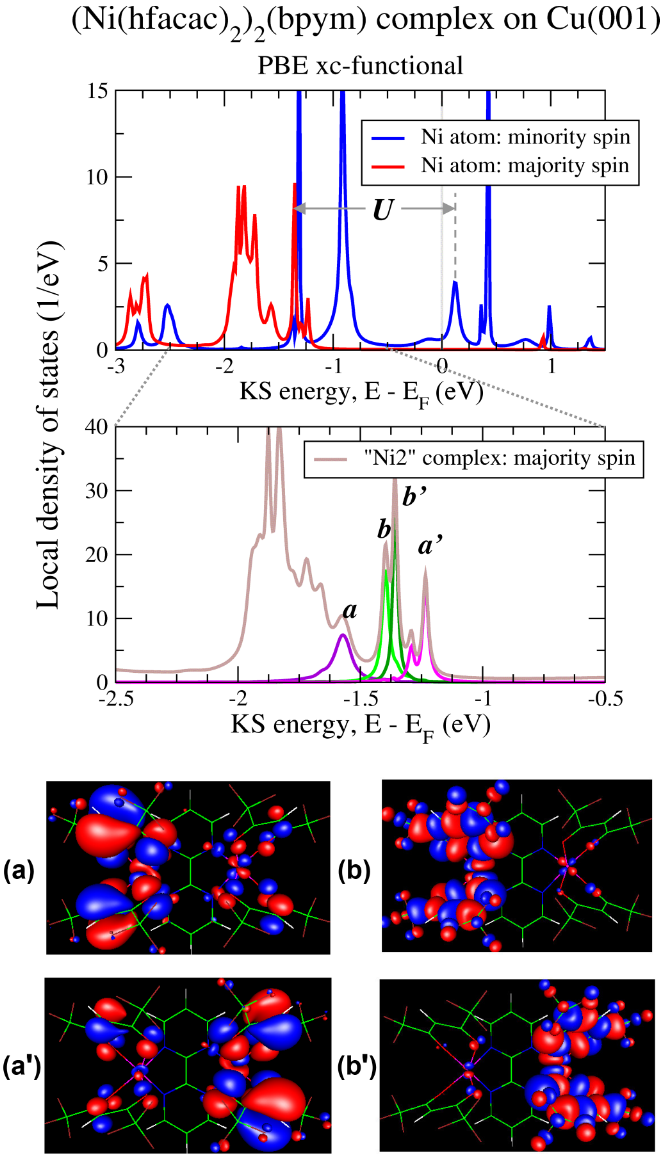

FIG. 7. (Color online) Upper plot: spin-dependent local density of states projected on one of the Ni atoms of the distorted $Ni_2$ complex deposited on Cu(001) [for a geometrical arrangement, see Fig. 6(g)]. Middle (zoomed in) plot shows majority (up-) spin spectral function below the Fermi level, where contributions are highlighted arising from four orbitals ($a$, $b$, $a'$, and $b'$), each carrying one unpaired spin. Corresponding wave functions are presented below. There $a$ and $b$ are localized on the left-hand side, while $a'$ and $b'$ are localized on the right-hand side of the molecular complex.

be incompatible with the Kondo effect observed experimentally), each subsystem will undergo Kondo screening independently below the Kondo temperature. We note that due to the inversion center, each spin has its own conduction channel [73]. Using Eq. (4) (limit $U \gg \varepsilon_d$), and parameters read from the computed spectral function (see Fig. 7),

$$2\Gamma^* = \Gamma_{a,a'} \simeq 0.1\ \text{eV} \gg \Gamma_{b,b'},$$

$$\varepsilon_d \sim 0.06\text{–}0.125\ \text{eV}, \quad U \simeq 1.5\ \text{eV} \gg \varepsilon_d,$$

we estimate $T_K \sim 0.4$–20 K, where the upper limit is above $J_{AF}$ and is in the range of experimental values.

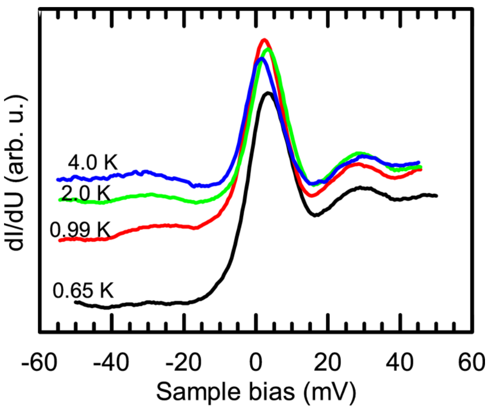

FIG. 8. (Color online) Differential conductance $dI/dU$ of $Ni_2$-$\beta$ measured at different temperatures. Sidebands at 30 mV are surrounding the Kondo resonance at zero bias. Feedback conditions: $U = 50$ mV, $I = 1$ nA, 2 mV modulation.

### D. Satellites accompanying the Kondo resonance

Yet another intriguing experimental observation, found in the differential conductance $dI/dU$ of $Ni_2$-$\beta$, are two satellites at ±30 mV (Fig. 8). We discuss further four possible hypotheses, which might explain their origin. These are (a) parallel conduction through frontier molecular orbitals (LUMOs); (b) low-energy magnetic excitations from the singlet ground state within the binuclear complex; (c) zero-field splitting of the triplet state of $Ni^{2+}$ ion; and (d) low-energy vibrational excitations of the complex and associated with that phonon-assisted Kondo effect. According to the analysis presented below, three hypotheses, (a), (b), and (c), are likely to be ruled out in favor of hypothesis (d).

*Hypothesis (a).* The first plausible suggestion is that satellites in $dI/dU$ around the Kondo resonance may be attributed to the parallel conduction through the LUMO and LUMO+1 of a $Ni_2$ complex, as summarized in Fig. 9. A distorted gas-phase $Ni_2$ complex has almost degenerate LUMO and LUMO+1 levels (e.g., in the minority spin channel, if Ni spins are coupled ferromagnetically), with splitting $\Delta \simeq 0.08$ eV comparable with the required energy scale $2\,\delta E \simeq 0.06$ eV. A pair of LUMO and LUMO+1 wave functions [see Fig. 9(c)] involve $d$ orbitals of two $Ni^{2+}$ centers hybridized via $\pi$ states of the central bpym unit. When the $Ni_2$ complex is deposited on a Cu surface (Fig. 6), molecular orbitals hybridize with the substrate states in different ways [72], as seen from Figs. 9(a) and 9(b). Two "satellites" are seen in the DFT spectral function $A(E)$: below $E_F$ (a "shoulder" of the partially occupied LUMO state) and above $E_F$ (mainly, LUMO+1 resonance) [74]. However, these satellites are placed at energies around ±100 meV vs the Fermi level, i.e., above the required energy $\delta E \simeq 30$ meV. Their positions in the spectral function $A(E)$ are furthermore sensitive to the variations in the absorption geometry [cf. Figs. 9(a) and 9(b)], and it is unlikely that the found satellites are always expected at equidistant points with respect to the Fermi level.

*Hypothesis (b).* Following the data presented in Table I, also magnetic excitations are unlikely to be the cause. A transition from AF to F coupling of $S = 1$ spins happens at the energy scale ~2 meV, too small to explain peaks at ±30 meV.

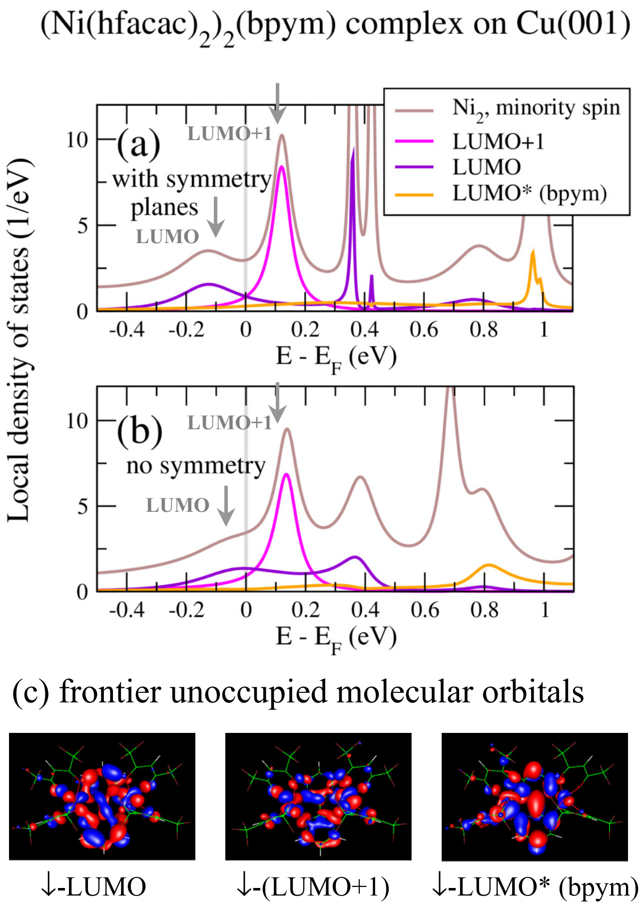

FIG. 9. (Color online) (a) and (b) Kohn-Sham spectral function of Ni$_2$ complex at Cu surface in the minority spin channel: (a) Ni$_2$ complex with local $C_{2v}$ symmetry; (b) Ni$_2$ complex relaxed at surface without symmetry constrains. Lower plot (c) shows frontier (minority-spin) unoccupied molecular orbitals.

Furthermore, the AF singlet ground state is not compatible with the observed Kondo effect. Furthermore, breaking Hund's rule and flipping a 1/2 spin at the Ni$^{2+}$ center is too expensive ($\sim$0.5 eV; see Table I).

*Hypothesis (c).* relies on zero-field spitting of a triplet $S = 1$ state (we refer here to one of the magnetically almost isolated subsystem—a Ni(hfacac)$_2$ unit with a single Ni$^{2+}$ center). Because of spin-orbit interaction, the triplet splits into a (quasidegenerate) doublet and a singlet, with the lowest energy state to be dependent on the sign of the largest anisotropy constant $D$ in the zero-field spin Hamiltonian, $H_{ZF} = D[S_z^2 - S(S+1)/3] + E(S_x^2 - S_y^2)$. An experimental evidence exists, Ref. [75], that for example under a strong distortion of the octahedral symmetry splitting can be of a few meV. However, if $D > 0$, the ground state is singlet, while the doublet is accessible at nonzero bias voltages only corresponding to a split Kondo resonance, a situation that is not observed experimentally. Contrarily, if $D < 0$, the ground state is (almost) degenerate, provided $|E| \ll |D|$. At zero bias voltage a fluctuation from $S_z = 1$ to $S_z = -1$ is not easily possible, since $\Delta S_z = 2$ is not compatible with a spin-flip event by a single substrate electron with $\Delta m = 1$. In this situation, only a scattering event of second order involving two electrons can cause a Kondo effect, which would result in extremely low Kondo temperatures.

*Hypothesis (d).* Under applied bias voltage, a "hot" electron tunneling from the STM tip (or from the surface) through a molecule may release its energy via emitting a phonon before participating in the spin-flip scattering processes. Such an inelastic Kondo effect would manifest itself as a "copy" of the Kondo resonance in $dI/dU$, which is, however, shifted from zero bias to the energy of molecular vibration [76].

To verify this idea, we have performed quantum-chemistry calculations of the electron-phonon coupling matrix elements for the Ni$_2$ complex. To simplify our analysis, we have considered a distorted molecular conformation of Ni$_2$ with imposed $C_{2v}$ symmetry that closely resembles the atomic structure of the complex preoptimized nearby a Cu(001) surface [see Suppl. Figs. 1(b) and 4(a) in the Supplemental Material [35]].

To first order, molecular vibrations of two Ni(hfacac)$_2$ units can be considered independently, since these units are attached to the bpym moiety, which is strongly bound to the Cu surface. Therefore, we consider one of the Ni(hfacac)$_2$ units and define an "active" subspace limited to 15 atoms including one Ni$^{2+}$ ion and surrounding atoms in its vicinity (see Fig. 10). There "colored" atoms are allowed to vibrate, while all other "reservoir" atoms shown in gray are assumed (as an approximation) to have infinite masses: either because some of them are heavy trifluoromethyl CF$_3$ groups, or because other atoms are bound to the surface. Such an approximation provides us with a set of 45 well-defined vibrational frequencies $\omega_\mu$.

Further, we consider the wave function $\psi_K$ [Fig. 10(b)], which dominates in the scattering channel responsible for the Kondo effect (essentially, $\psi_K$ is one of those single-occupied

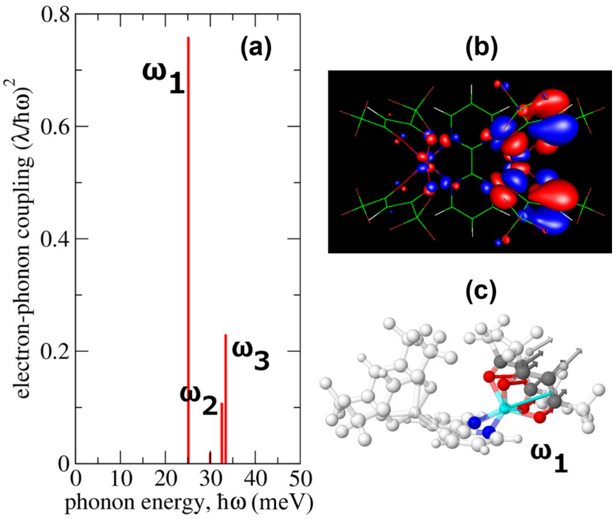

FIG. 10. (Color online) Dimensionless electron-phonon (*el-ph*) coupling constants (a) between the "Kondo-active" molecular orbital $\psi_K$ shown in (b) and low-energy vibrational eigenmodes, which are forced to be localized in the vicinity of Ni$^{2+}$ ion at the right-hand side of the molecule (see text for details). Plot (c) is a visual representation of the mode (atomic displacements are scaled by $\times 10$) with energy $\hbar\omega_1 = 25.1$ meV exhibiting the largest *el-ph* coupling constant $\approx$0.75.

molecular orbitals depicted as $a$ and $a'$ in Fig. 9, which strongly hybridize with the Cu surface) [77]. We have computed electron-phonon coupling matrix elements $\lambda^{\mu}$, involving the orbital $\psi_K$ and molecular vibrations, which are localized within the same active subspace (for computational details, see Supplemental Material [35], Sec. III).

Our results are presented in Fig. 10 in which we show the dimensionless electron-phonon coupling constants $g = (\lambda^{\mu}/\hbar\omega_{\mu})^2$ limited to the low-energy excitations. We observe only three eigenmodes (25.1, 32.6, and 33.4 meV) with nonzero coupling constants and frequencies in the proximity of $\delta E \simeq 30$ meV. Furthermore, we show in the Supplemental Material [35], Sec. III, that the eigenmodes involve vibrations of $Ni^{2+}$ ions. Their energies will be renormalized when coupled to a continuum of vibrational modes of the macroscopic system, including remaining functional groups of the molecular complex and the Cu surface. However, our additional calculations show that, for example, interaction between two Ni subsystems introduces a moderate splitting of the frequencies only, around ~0.5 meV. Thus, we argue that three vibrational eigenmodes may rationalize the observation of satellites in $dI/dU$ as a signature of the phonon-assisted Kondo effect.

## V. CONCLUSION

To summarize, low-temperature STS measurements on binuclear metal-organic complexes, $Ni_2$ and $Mn_2$, deposited on a Cu(001) surface revealed that the systems undergo the Kondo effect with the Kondo resonances located nearby transition-metal atoms. The relatively large Kondo temperatures, of the order of ~10 K, were found to depend on the adsorption type. The situation was intriguing here, because the synthesized molecules do not have predefined anchoring groups, which could be responsible for a formation of the chemical bond with the Cu surface [34].

We rationalized experimental observations by performing extensive density functional theory calculations. We searched for the adsorption geometries, where molecules are chemisorbed on the surfaces. In case of $Ni_2$, our simulations show that some STM images ($Ni_2$-$\beta$) can be attributed to a distorted $Ni_2$ complex with partially weakened internal chemical bonds, while other STM images ($Ni_2$-$\alpha$) may be interpreted as arising from molecular fragmentation. In both cases, our calculations suggest a picture of the underscreened ($S = 1$)-type Kondo effect emerging from the open $3d$ shells of the individual $Ni^{2+}$ ions. Furthermore, theoretical analysis points out that the satellites in the STS spectra observed nearby the zero-bias resonance are likely a signature of the low-energy vibrational excitations of the $Ni_2$ complex and associated with that phonon-assisted Kondo effect.

In broader terms, binuclear complexes present an excellent playground for studying fundamental aspects of magnetic two-impurity (or double quantum dot) systems. By functionalizing the bridging unit it could be possible to enhance the superexchange interaction between two centers, thus allowing us to access different regions of the phase diagram of the double impurity model [73,78,79]. On the applied level, understanding interaction between the spins residing on different functional units is vital to quantum information storage and processing with molecules assembled on surfaces. Our work provides an important step in this direction and identifies further challenges. Apart from the appealing enhancement of the superexchange, the substitution of Ising-like spins (such as Tb) may offer means to study a "double molecular magnet." As demonstrated here, first-principles calculations will play an indispensable role in this effort.

## ACKNOWLEDGMENTS

We thank K. Fink for fruitful discussions and M. Bürkle for providing us with a development version of the TURBOMOLE package. A.B. acknowledges support of Deutsche Forschungsgemeinschaft (DFG) through the Research Grant No. BA 4265/2-1. W.W. and M.R. acknowledge support from the French-German University and Baden-Württemberg Stiftung in the framework of the Kompetenznetz für Funktionale Nanostrukturen (KFN). D.X. and M.A. acknowledge computational resources from HPC Méso Centre of the Strasbourg University and GENCI-CINES Grant No. 2014-gem1100.

---

[1] J. Reichert, R. Ochs, D. Beckmann, H. B. Weber, M. Mayor, and H. v. Löhneysen, Phys. Rev. Lett. **88**, 176804 (2002).

[2] M. Elbing, R. Ochs, M. Koentopp, M. Fischer, C. von Hänisch, F. Weigend, F. Evers, H. B. Weber, and M. Mayor, Proc. Natl. Acad. Sci. USA **102**, 8815 (2005).

[3] J. Park, A. N. Pasupathy, J. I. Goldsmith, C. Chang, Y. Yaish, J. R. Petta, M. Rinkoski, J. P. Sethna, H. D. Abruña, P. L. McEuen, and D. C. Ralph, Nature (London) **417**, 722 (2002).

[4] S. Kubatkin, A. Danilov, M. Hjort, H. Cornil, J.-L. Brédas, N. Stuhr-Hansen, P. Hedegård, and T. Bjørnholm, Nature (London) **425**, 698 (2003).

[5] E. A. Osorio, K. O'Neill, N. Stuhr-Hansen, F. Nielsen, T. Bjørnholm, and H. S. J. van der Zant, Adv. Mater. **19**, 281 (2007).

[6] E. Lörtscher, J. W. Ciszek, J. Tour, and H. Riel, Small **2**, 973 (2006).

[7] V. Meded, A. Bagrets, A. Arnold, and F. Evers, Small **5**, 2218 (2009).

[8] S. Schmaus, A. Bagrets, Y. Nahas, T. K. Yamada, A. Bork, M. Bowen, E. Beaurepaire, F. Evers, and W. Wulfhekel, Nat. Nanotechnol. **6**, 185 (2011).

[9] A. Bagrets, S. Schmaus, A. Jaafar, D. Kramczynski, T. K. Yamada, M. Alouani, W. Wulfhekel, and F. Evers, Nano Lett. **12**, 5131 (2012).

[10] P. Gütlich, Y. Garcia, and H. A. Goodwinb, Chem. Soc. Rev. **29**, 419 (2000).

[11] V. Meded, A. Bagrets, K. Fink, R. Chandrasekar, M. Ruben, F. Evers, A. Bernand-Mantel, J. S. Seldenthuis, A. Beukman, and H. S. J. van der Zant, Phys. Rev. B **83**, 245415 (2011).

[12] I. Beljakov, V. Meded, F. Symalla, K. Fink, S. Shallcross, M. Ruben, and W. Wenzel, Nano Lett. **14**, 3364 (2014).

[13] J. Li, W.-D. Schneider, R. Berndt, and B. Delley, Phys. Rev. Lett. **80**, 2893 (1998).

[14] V. Madhavan, W. Chen, T. Jamneala, M. F. Crommie, and N. S. Wingreen, Science **280**, 567 (1998).

[15] H. C. Manoharan, C. P. Lutz, and D. M. Eigler, Nature (London) **403**, 512 (2000).

[16] N. Knorr, M. A. Schneider, L. Diekhöner, P. Wahl, and K. Kern, Phys. Rev. Lett. **88**, 096804 (2002).

[17] N. Néel, J. Kröger, L. Limot, K. Palotas, W. A. Hofer, and R. Berndt, Phys. Rev. Lett. **98**, 016801 (2007).

[18] D. Ehm, S. Hüfner, S. F. Reinert, J. Kroha, P. Wölfle, O. Stockert, C. Geibel, and H. v. Löhneysen, Phys. Rev. B **76**, 045117 (2007).

[19] L. Gao, W. Ji, Y. B. Hu *et al.*, Phys. Rev. Lett. **99**, 106402 (2007).

[20] Y.-S. Fu, S.-H. Ji, Xi Chen *et al.*, Phys. Rev. Lett. **99**, 256601 (2007).

[21] I. Fernández-Torrente, K. J. Franke, and J. I. Pascual, Phys. Rev. Lett. **101**, 217203 (2008).

[22] U. G. E. Perera, H. J. Kulik, V. Iancu, L. G. G. V. Dias da Silva, S. E. Ulloa, N. Marzari, and S.-W. Hla, Phys. Rev. Lett. **105**, 106601 (2010).

[23] J. Nygård, D. H. Cobden, and P. E. Lindelof, Nature (London) **408**, 342 (2000).

[24] J. Paaske, A. Rosch, P. Wölfle, N. Mason, C. M. Marcus, and J. Nygård, Nat. Phys. **2**, 460 (2006).

[25] Single molecule magnets (SMMs) have attracted a lot of interest [26,27] recently. For example, magnetic relaxation time of SMMs could be years at low temperatures that has been observed in bulk crystals [28,29]. Potential applications of SMMs, e.g., as high-density data storage units, are envisaged. For that, individual molecular magnets need to be deposited onto supportive substrates where, due to hybridization effects, a possibility exists for surface induced changing in magnetic coupling and anisotropy. There is still a lack of clear understanding on how magnetic properties of SMMs are altered by absorption. While in the earlier studies magnetic nature of supported molecular magnets has not been demonstrated [30], recent works on Tb(III) [31] and $\mathrm{Mn}_{12}$ complexes [32] seem to confirm that the SMM character at the surface may be preserved.

[26] D. Gatteschi and R. Sessoli, Angew. Chem. Int. Ed. **42**, 268 (2003).

[27] L. Bogani and W. Wernsdorfer, Nat. Mater. **7**, 179 (2008).

[28] G. Christou, D. Gatteschi, D. N. Hendrickson, and R. Sessoli, Mater. Res. Soc. Bull. **25**, 66 (2000).

[29] M. Cavallini, M. Facchini, C. Albonetti, and F. Biscarini, Phys. Chem. Chem. Phys. **10**, 784 (2008).

[30] J. Gómez-Segura, I. Díez-Pérez, N. Ishikawa, M. Nakano, J. Vecianaa, and D. Ruiz-Molina, Chem. Commun. **27**, 2866 (2006).

[31] L. Vitali, S. Fabris, A. M. Conte, S. Brink, M. Ruben, S. Baroni, and K. Kern, Nano Lett. **8**, 3364 (2008).

[32] S. Kahle, Zh. Deng, N. Malinowski, Ch. Tonnoir, A. Forment-Aliaga, N. Thontasen, G. Rinke, D. Le, V. Turkowski, T. S. Rahman, S. Rauschenbach, M. Ternes, and K. Kern, Nano Lett. **12**, 518 (2012).

[33] W. Liang, M. P. Shores, M. Bockrath, J. R. Long, and H. Park, Nature (London) **417**, 725 (2002).

[34] S. Wagner, F. Kisslinger, S. Ballmann, F. Schramm, R. Chandrasekar, T. Bodenstein, O. Fuhr, D. Secker, K. Fink, M. Ruben, and H. B. Weber, Nat. Nanotechnol. **8**, 575 (2013).

[35] See Supplemental Material at http://link.aps.org/supplemental/10.1103/PhysRevB.91.195424 for details of electronic structure calculations and synthesis of molecular complexes, which includes Refs. [36–45].

[36] A. Schäfer, H. Horn, and R. Ahlrichs, J. Chem. Phys. **97**, 2571 (1992).

[37] K. Eichkorn, O. Treutler, H.Öhm, M. Häser, and R. Ahlrichs, Chem. Phys. Lett. **242**, 652 (1995).

[38] J. Tersoff and D. R. Hamann, Phys. Rev. B **31**, 805 (1985).

[39] P. Deglmann, K. May, F. Furche, and R. Ahlrichs, Chem. Phys. Lett. **384**, 103 (2004).

[40] P. Deglmann, F. Furche, and R. Ahlrichs, Chem. Phys. Lett. **362**, 511 (2004).

[41] P. Deglmann and F. Furche, J. Chem. Phys. **117**, 9535 (2002).

[42] M. Bürkle, J. K. Viljas, T. J. Hellmuth, E. Scheer, F. Weigend, G. Schön, and F. Pauly, Phys. Status Solidi B **250**, 2468 (2013).

[43] G. M. Sheldrick, A short history of SHELX. Acta Crystallogr., Sect. A **64**, 112 (2008).

[44] G. M. Sheldrick, *SHELXTL97-2* (University of Göttingen, Germany, 1997).

[45] G. A. Bain and J. F. Berry, J. Chem. Educ. **85**, 532 (2008).

[46] A listing of data collection and refinement procedures as well as positional coordinates of all atoms (CIF files) were deposited at the Cambridge Crystallographic Data Centre under CCDC-1023858 for $[(\mathrm{Ni(hfacac)_2})_2(\mathrm{bpym})]^0$, and CCDC-1023859 for $[(\mathrm{Mn(hfacac)_2})_2(\mathrm{bpym})]^0$, respectively, which contain the supplementary crystallographic data excluding structure factors. These data can be obtained free of charge via www.ccdc.cam.ac.uk/conts/retrieving.html [or from the Cambridge Crystallographic Data Centre, 12, Union Road, Cambridge CB2 1EZ, UK; FAX: (+44) 1223-336-033; or deposit@ccdc.cam.ac.uk].

[47] M. Barquín, M. J. G. Garmendia, and V. Bellido, Trans. Met. Chem. **24**, 546 (1999).

[48] G. Brewer and E. Sinn, Inorg. Chem. **24**, 4580 (1985).

[49] V. Blum, R. Gehrke, F. Hanke, P. Havu, V. Havu, X. Ren, K. Reuter, and M. Scheffler, Comput. Phys. Commun. **180**, 2175 (2009).

[50] R. Ahlrichs *et al.*, TURBOMOLE 6.6 (development version), program package for *ab initio* electronic structure calculations, Turbomole GmbH, 2014, http://www.turbomole.com/

[51] L. Zhang, T. Miyamachi, T. Tomani, R. Dehm, and W. Wulfhekel, Rev. Sci. Instrum. **82**, 103702 (2011).

[52] J. Kondo, Prog. Theor. Phys. **32**, 37 (1964).

[53] L. Kouwenhoven and L. Glazman, Phys. World **14**, 33 (2001).

[54] U. Fano, Phys. Rev. **124**, 1866 (1961).

[55] O. Újsághy, J. Kroha, L. Szunyogh, and A. Zawadowski, Phys. Rev. Lett. **85**, 2557 (2000).

[56] J. Merino and O. Gunnarsson, Phys. Rev. B **69**, 115404 (2004).

[57] M. Plihal and J. W. Gadzuk, Phys. Rev. B **63**, 085404 (2001).

[58] K. Nagaoka, T. Jamneala, M. Grobis, and M. F. Crommie, Phys. Rev. Lett. **88**, 077205 (2002).

[59] P. W. Anderson, Phys. Rev. **124**, 41 (1961).

[60] A. C. Hewson, *The Kondo Problem to Heavy Fermions*, Cambridge Studies in Magnetism, Band 2 (Cambridge University Press, Cambridge, England, 1993).

[61] The formula for the Kondo temperature reads as $k_B T_\mathrm{K} \simeq 0.41U\sqrt{\frac{\Gamma}{4U}}e^{-\pi(U-\varepsilon_d)\varepsilon_d/U\Gamma}$, where $-\varepsilon_d < 0$ is a position of the occupied resonance level measured vs Fermi energy, $\Gamma$ is the resonance width, and $U$ is the Coulomb on-site interaction.

[62] A. Tkatchenko and M. Scheffler, Phys. Rev. Lett. **102**, 073005 (2009).
[63] G. Kresse and J. Furthmüller, Phys. Rev. B **54**, 11169 (1996).
[64] A. Arnold, F. Weigend, and F. Evers, J. Chem. Phys. **126**, 174101 (2007).
[65] J. Wilhelm, M. Walz, M. Stendel, A. Bagrets, and F. Evers, Phys. Chem. Chem. Phys. **15**, 6684 (2013).
[66] T. Jamneala, V. Madhavan, W. Chen, and M. F. Crommie, Phys. Rev. B **61**, 9990 (2000).
[67] J. P. Perdew, K. Burke, and M. Ernzerhof, Phys. Rev. Lett. **77**, 3865 (1996).
[68] V. I. Anisimov, F. Aryasetiawan, and A. I. Lichtenstein, J. Phys.: Condens. Matter **9**, 767 (1997).
[69] S. Kümmel and L. Kronik, Rev. Mod. Phys. **80**, 3 (2008).
[70] S. L. Dudarev, G. A. Botton, S. Y. Savrasov, C. J. Humphreys, and A. P. Sutton, Phys. Rev. B **57**, 1505 (1998).
[71] A. Bagrets, J. Chem. Theory Comput. **9**, 2801 (2013).
[72] Our calculations indicate that a fractional charge of $\approx 0.5e$ leaks out from the surface to the molecule, populating partially the LUMO of the $\mathrm{Ni}_2$ complex and the LUMO* of the bpym moiety (see Fig. 9). Also, a magnetic moment carried by the complex is slightly reduced, from $4.0\mu_B$ (gas-phase molecule) down to $3.3\mu_B$.
[73] C. Jayaprakash, H. R. Krishna-murthy, and J. W. Wilkins, Phys. Rev. Lett. **47**, 737 (1981).
[74] We remind that DFT with a quasilocal XC functional does not allow us to recover a Kondo resonance at the Fermi level.
[75] J. J. Parks, A. R. Champagne, T. A. Costi, W. W. Shum, A. N. Pasupathy, E. Neuscamman, S. Flores-Torres, P. S. Cornaglia, A. A. Aligia, C. A. Balseiro, G. K.-L. Chan, H. D. Abruña, and D. C. Ralph, Science **328**, 1370 (2010).
[76] J. Paaske and K. Flensberg, Phys. Rev. Lett. **94**, 176801 (2005).
[77] More specifically, "Kondo-active" molecular orbitals (MOs) depicted as $a$ and $a'$ in Fig. 9, which are strongly coupled to the Cu surface, are well approximated by symmetric and antisymmetric combinations $\psi_K^{\pm} = \frac{1}{\sqrt{2}}(\phi_{b_1}^{\uparrow} \pm \phi_{a_2}^{\uparrow})$ of the single-occupied MOs of the distorted $\mathrm{Ni}_2$ complex with $C_{2v}$ symmetry. Here $b_1$ and $a_2$ refer to irreducible representations of the $C_{2v}$ group, with $b_1$ being even and $a_2$ being odd with respect left-right reflection $\sigma_v$.
[78] W. Hofstetter and H. Schoeller, Phys. Rev. Lett. **88**, 016803 (2001).
[79] J. Bork, Y.-h. Zhang, L. Diekhöner, L. Borda, P. Simon, J. Kroha, P. Wahl, and K. Kern, Nat. Phys. **7**, 901 (2011).